Effect of SiO$_2$ flux on the depth of penetration, microstructure, texture and mechanical behavior of AA6063 T6 aluminum alloy using activated TIG welding

Rajiv KUMAR[1], S.C. VETTIVEL[2]*, and Harmesh KUMAR KANSAL[1]

[1] Department of Mechanical Engineering, UIET, Panjab University, Chandigarh, India
[2] Department of Mechanical Engineering, Chandigarh College of Engineering and Technology (Degree Wing), Chandigarh, India

Abstract. Activated tungsten inert gas (ATIG) welding has a good depth of penetration (DOP) as compared to the conventional tungsten inert gas (TIG) welding. This paper is mainly focused on ATIG characterization and mechanical behavior of aluminum alloy (AA) 6063-T6 using SiO$_2$ flux. The characterization of the base material (BM), fusion zone (FZ), heat affected zone (HAZ) and, partially melted zone is carried out using the suitable characterization methods. The weld quality is characterized using ultrasonic-assisted non-destructive evaluation. A-scan result confirms that the ATIG welded samples have more DOP and less bead width as compared to conventional TIG. The recorded tensile strength of ATIG with SiO$_2$ is better than the conventional TIG welding. The failure mode is ductile for ATIG welding with larger fracture edges and is brittle in the case of conventional TIG welding.

Key words: aluminum alloy; depth of penetration; tensile strength; texture.

1. Introduction

Aluminium alloy (AA) 6063 has good mechanical properties like strength, corrosion resistance and toughness [1]. The AA6063 is used in marine industry, automobile industry, medical equipment, and aircraft applications [2–4].

In tungsten inert gas (TIG) welding the electric arc is generated between a non-consumable tungsten electrode and the metal to be welded. Weld pool is generated by part of the heat produced by the electric arc [5]. The welding area near the pool is protected by inert gases [6–8]. When modified to increase the depth of penetration and productivity with activating fluxes, TIG is called activated TIG (ATIG). ATIG welding is effective enough and produces high quality welding joints more efficiently than conventional TIG [9].

In ATIG welding process, a thin layer of flux is pasted on the location of the welding. The mixture paste is prepared mixing flux with a solvent and TIG welding is done with a filler. ATIG welding joints showed a good improvement in the DOP as compared to the conventional TIG [10].

Hemant et al. [11] used many oxide fluxes like Cr$_2$O$_3$, FeO, Fe$_2$O$_3$, MoO$_3$, SiO$_2$, and Al$_2$O$_3$ to find the welding properties in stainless steel welded joints. The results confirmed that there was an increase in the DOP. Vidyarthy et al. [8, 9, 12] confirmed that mechanical properties like hardness, impact, strength, etc. were better as compared to conventional TIG.

Many researchers have investigated the effect of fluxes on mechanical properties on ATIG welded joints. But very minimal investigation and study is done on the grain size and texture in ATIG-welded AA joints using electron backscatter diffraction (EBSD). In present study of mechanical properties, microstructure, and texture of AA 6063 T6 using ATIG with flux SiO$_2$ are investigated. Trials are conducted to select the welding parameters as explained in [13–18].

2. Materials and methods

2.1. Materials. In present research the base metal chosen is AA6063-T6 aluminum alloy. The dimensions for base material flat of AA6063 T6 purchased from Mallinath Metal, Mumbai, Maharashtra, India are 1000*300*6 mm. The composition and mechanical properties of the AA6063-T6 are listed in Table 1 and the filler wire is presented in Table 2. The AA6063-T6 and filler AA 5356 are purchased from Mallinath Metal, Mumbai, Maharashtra, India.

Table 1
AA 6063 T6 Chemical composition

Element	Al	Si	Cu	Mn	Mg	Cr	Fe	Zn
Wt.%	97.9	0.2	0.1	0.1	0.7	0.1	0.35	0.1

Table 2
Filler Rod AA 5356 Chemical composition

Element	Al	Si	Fe	Cu	Ti	Zn	Mn	Mg
Wt.%	Bal	0.2	0.4	0.1	0.2	0.1	0.1	4.5

*e-mail: scvettivel@ccet.ac.in

Bull. Pol. Ac.: Tech. 69(1) 2021, e136215

1

2.2. Activation flux. The SiO_2 flux has been selected for this study. The quantity of flux used per sample is $3-4 * 10-2 \ mg/mm^2$. The oxide flux is purchased from Akshar Exim Company Private Limited, Kolkata, West Bengal, India. The chemical composition of the SiO_2 flux is listed in Table 3.

Table 3
Chemical compositions of the SiO_2 flux

Molecular formula	Density g/cm³	Melting point °C	Boiling point °C	Molecular weight g/mol
SiO_2	2.3	1710	2230	60.083

2.3. Preparation of flux paste. The preparation of flux paste is one of the most important tasks in ATIG welding. The quantity of the flux needed is calculated as explained in [7, 9] and given in Eqs. (1) and (2). In this work, 160 mm long, 12 mm wide, and 0.2 mm thick layers are deposited as shown in Fig. 1.

$$m = \rho * v, \qquad (1)$$

where: ρ is density of the flux,
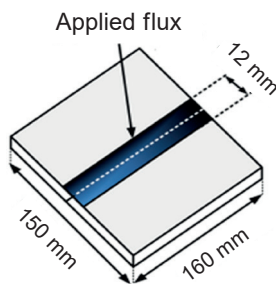v is volume of the area to be welded.

Fig. 1. Applied flux surface

Also,

$$v = l * w * t, \qquad (2)$$

where: l is length of the weld,
w is width of weld,
t is thickness of the weld.
A paste of SiO_2 flux was prepared with the help of acetone, which was added in proportion 7–9 ml/g. After the preparation of the flux paste, it was applied just before ATIG welding as presented in Fig. 1.

2.4. ATIG welding. In present work, a 6-mm thick plate was cut into 160×75 mm. The metal piece to be welded is prepared by removing top surface impurities and irregularities by using grinding followed by cleaning with acetone. A suitable arc length was adjusted to 3–3.5 mm between the electrode tip and workpiece. The welding was carried out at 115 mm/min. ATIG welding power source (Make: Panasonic, Model BR1–200

(AC/DC), capacity: 250 A with machine torch) with standard argon gas with the regulator was used for welding. A standard thoriated tungsten electrode rod with a diameter of 3 mm was used in welding. The argon gas was applied to cover the weld pool. The constant electrode gap was maintained to make sure that the welding was being done under similar conditions. The important welding variables are as shown in Table 4.

Table 4
Welding parameters

Welding current, Amps	Welding speed, mm/min	Arc length, mm	Shielding gas, l/min	Electrode dia. mm
160–230	115	3–3.5	Argon (99.99%)	3

2.5. Non-destructive evaluation. Ultrasonic non-destructive evaluation (NDE) using A-scan examination was carried out on the weldment.

2.6. Tensile test. The ultimate tensile strength of the conventional TIG and ATIG was studied through a tensile testing at CITCO, Industrial Area, Chandigarh, India on FIE MAKE Universal Testing Machine. The samples were prepared using electrical discharge machining (wire cut) as per ASTM E-8M standard as shown in Fig. 2. The data was analysed for each specimen and the mean value was recorded.
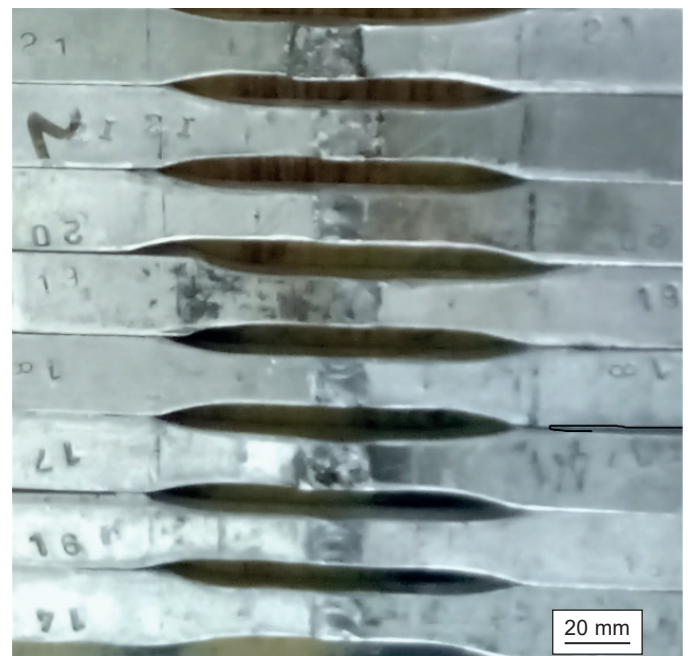

Fig. 2. Tensile test specimen

2.7. Characterization. A mounting press is used to prepare and polish the samples by using different grit sizes varying from 50 to 3000. The alumina and diamond paste along with the velvet

2

Bull. Pol. Ac.: Tech. 69(1) 2021, e136215

cloth is used to smooth the surface of the specimen at Chandigarh College of Engineering Technology (Degree Wing), Chandigarh, India. The samples were etched with Keller's reagent after polishing to view the microstructure with help of the optical microscope (RADICAL, model RXM 7). A field emission gun scanning electron microscopy (FEGSEM) (Model: JEOL JSM 7600F) and energy dispersive spectroscopy (EDS) at the Indian Institute of Science Education and Research Mohali, Panjab, India is used to study sample before and after fracture. The EBSD texture analysis is done by FEI Quanta TM Nova Nano SEM, A TSL-OIM^{TM} EBSD system at IIT Bombay. The samples are prepared after electro-polishing with the help of 80:20 methanol: Per Chloric acid, 13 V dc and-20°C. Areas of 500 μm by 500 μm were scanned at 0.5 μm step size for each welded sample at weldment.

3. Results and discussion

3.1. Depth of penetration and quality of the weld. To evaluate and investigate the quality of ATIG welding and DOP, the trial testing ATIG with flux is carried out from 160–230 A. The following results were reported. The DOP below 175 A was not good and burning of metal was observed at the weldments at or above 220 A. It is concluded that the full DOP without any major defects identified below 220 A. Figure 3 shows the DOP, width of the bead, and ultrasonic scan results of the conventional TIG and ATIG welded with SiO$_2$ at 200 A. Figures 3a and 3d showed the sectional view showing DOP of

conventional TIG and ATIG with SiO$_2$ and the effect of flux on bead width is shown in Figs. 3b and 3e. Figures 3a, 3b, 3d and 3e confirmed that in conventional TIG-welded samples the bead width is more than ATIG. Figures 3c and 3f confirmed that DOP is less in conventional TIG as compared to the ATIG using flux SiO$_2$. The reason for increased DOP in ATIG welding is due to a high surface tension gradient at the outer periphery of the weld pool as compared to the centre of the weld pool. The second reason is that in ATIG welding oxide flux is melted in the weld zone and oxygen was released from the flux. The excess amount of oxygen from the flux increase the heat input. As a result DOP increased as compared to conventional TIG welding where the entrapment of oxygen is restricted by using the shielding gas [16]. Figures 3b and 3c showed that the recorded bead width is 16 mm and DOP is 4.7 mm, which is not full depth. The DOP of ATIG welded AA 6063-T6 with filler rod AA5356 and flux SiO$_2$ is shown in Figs. 3d and 3f. It showed that there is a gain in DOP due to the use of flux SiO$_2$. It was also confirmed by Figs. 3d and 3f that full depth of penetration with minimum bead width 6 mm is achieved in ATIG without any defects.

3.2. OM characterization. Figure 4 showed that the optical OM images at 400× of the BM, FZ, and interface for conventional TIG and ATIG welded joints using flux (SiO$_2$). The weldment is divided into three different zones as per the temperature gained during welding by workpiece. They are the FZ, partially melted zone (PMZ), and HAZ. Figure. 4b and 4d show the OM of the images of FZ the conventional TIG and ATIG
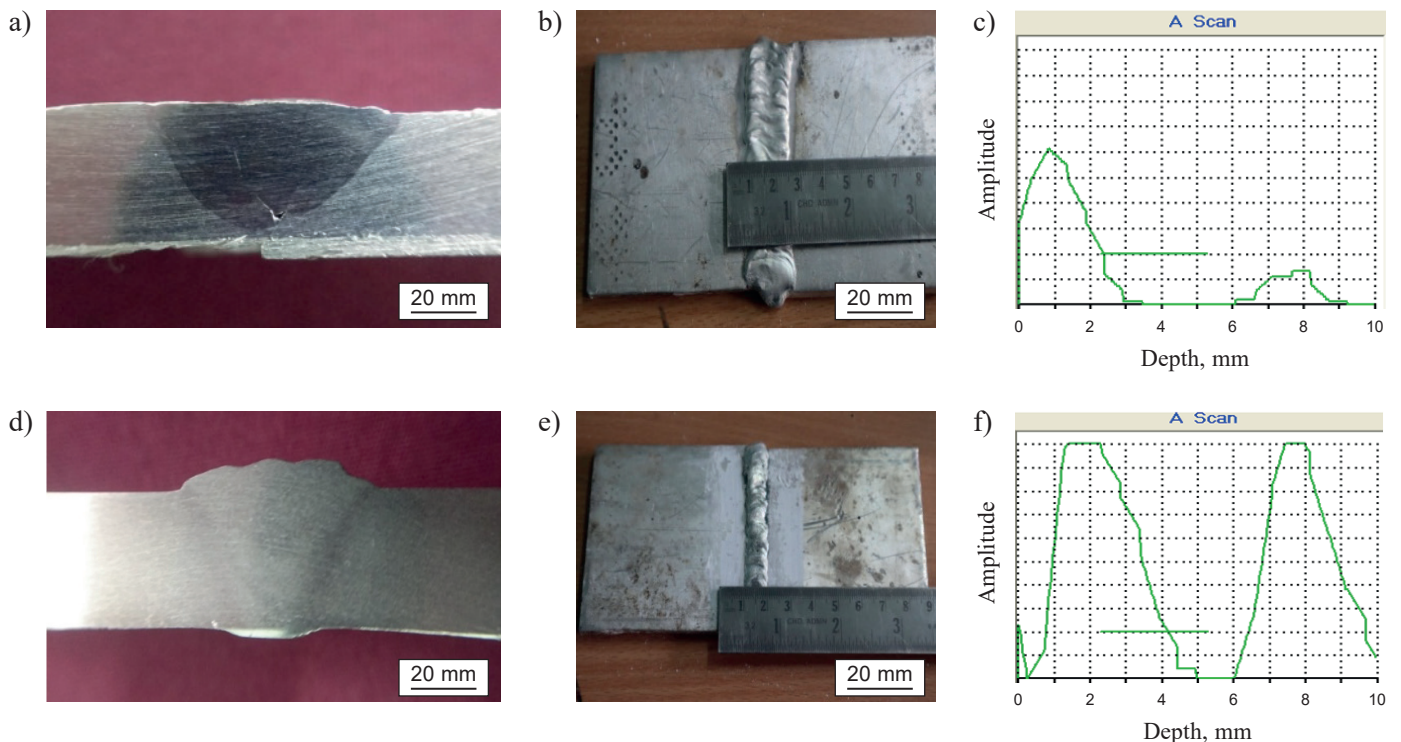

Fig. 3. DOP, bead width and ultrasonic A-scan of conventional TIG and ATIG welded samples: a) DOP of conventional TIG; b) width of conventional TIG; c) A-scan of conventional TIG; d) DOP of ATIG using SiO$_2$; e) width of ATIG using SiO$_2$; f) A scan of ATIG using SiO$_2$

Bull. Pol. Ac.: Tech. 69(1) 2021, e136215
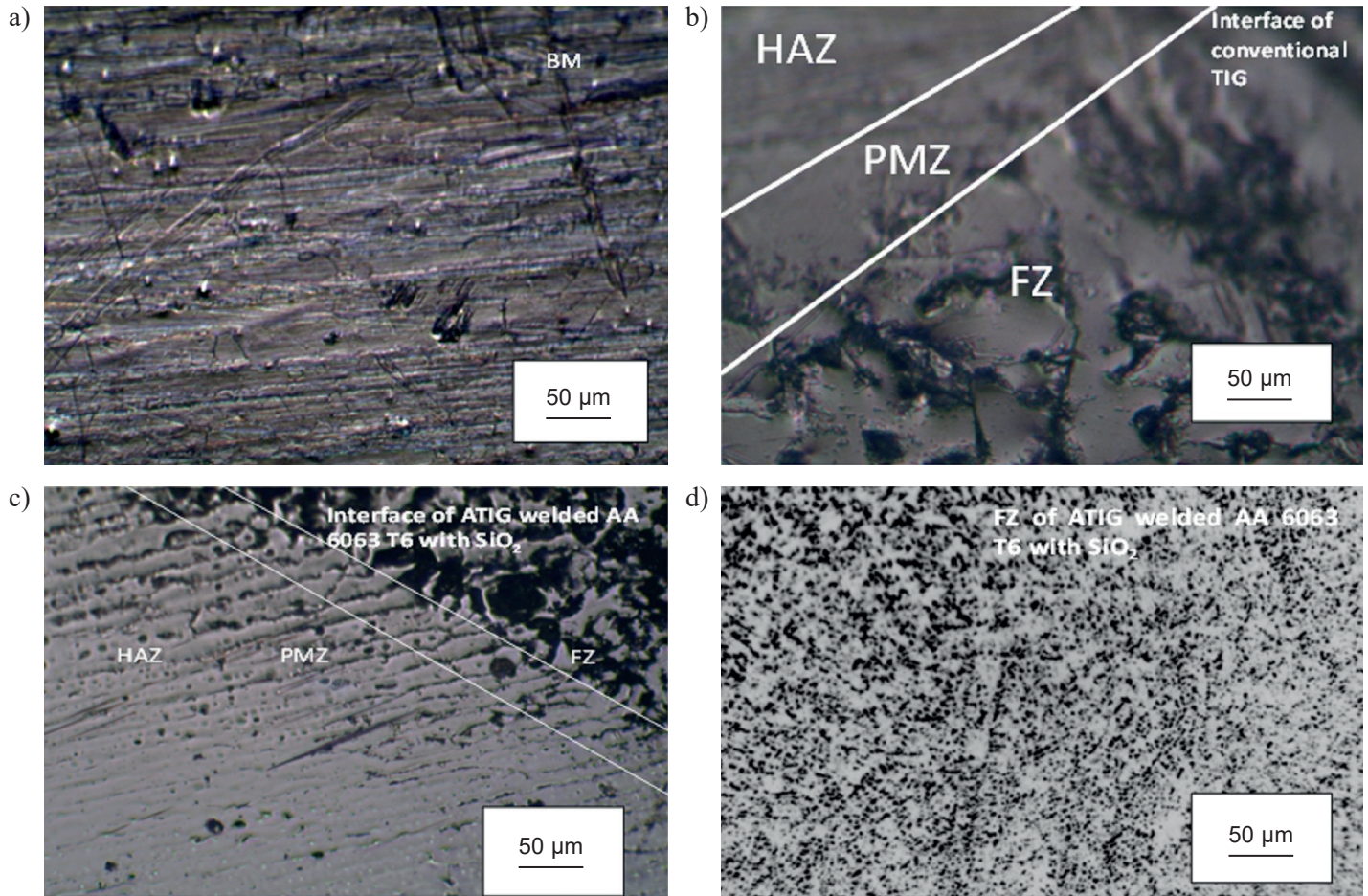
3

a)

b)

c)

d)

Fig. 4. OM images of AA 6063-T6 with conventional TIG and ATIG: a) BM, b) FZ of conventional TIG, c) interface of ATIG using SiO$_2$, d) FZ of ATIG using SiO$_2$

welded joints. The microstructure at PMZ of ATIG weldment of AA6063-T6 is shown in Fig. 4c.

In Figs. 4b and 4d, dendrites and column dendrites were observed in the FZ of each sample. This happened due to fast heating and cooling in FZ at the time of the welding. The only difference noticed in FZ is spacing in dendrite arms.

A finer microstructure is observed in ATIG with flux SiO$_2$ and coarse microstructure in the conventional TIG welded joints as confirmed by Figs. 4b and 4d. This is mainly due to spacing in the dendrite arms. A random disorientation between BM grains and FZ boundary grains is noticed as shown in Fig. 4c. The microstructure in the FZ depends on the solidification behavior of the weld pool [13, 14]. The PMZ is region of the HAZ where the peak temperature crossed the equilibrium solidus temperature [12]. Figure 4c confirmed that the microstructure varies towards the center of the weld from FZ boundary because the temperature gradient is towards the direction weld pool center. Therefore, the grains have a maximum probability to solidify towards the fusion line. The size of the grains in HAZ of ATIG is less as compared to conventional TIG. Also, at the high-temperature the Mg$_2$Si phase precipitate and grows up in the HAZ and resulted in the softening of HAZ which deteriorates the mechanical properties [14].

3.3. SEM-EDS analysis. SEM-EDS mapping was used to evaluate and characterize the BM and welding joints of conventional TIG, and ATIG with flux (SiO$_2$) as shown in Fig. 5. The SEM & EDS analysis of BM AA 6063-T6 is presented in Figs. 5a and 5b. The various elements identified are Si, Zn, Mg, Cu, Ni, Ti, Fe, and Cr. The major element confirmed in AA 6063-T6 is Mg and Si. It is also noted that there was no strong variation in the composition of the FZ of all ATIG welded samples with flux (SiO$_2$) and BM as shown in Figs. 5a and 5b and Figs. 5c and 5d. Figures 5c and 5d is the SEM-EDS map of ATIG with flux SiO$_2$. Typical inter-granular precipitates of Fe, Mg, and Si are identified. The EDS map analysis represents that nuclei are rich in Si, Ti, and Mg. There is no change in the content of Mn, Zn, Cu, Ti, Zr after welding. But the content of Mg and Si was increased slightly due to the use of a filler rod AA5356. It is concluded that ATIG welding did not have to change the elemental composition of FZ than Mg and Si [16].

3.4. Texture analysis by EBSD. In this work a quantitative and systematic analysis of the inverse pole figures (IPFs) done to study the distribution of microstructure. The shape and size of grain increases from the boundary to the FZ line in the direc-
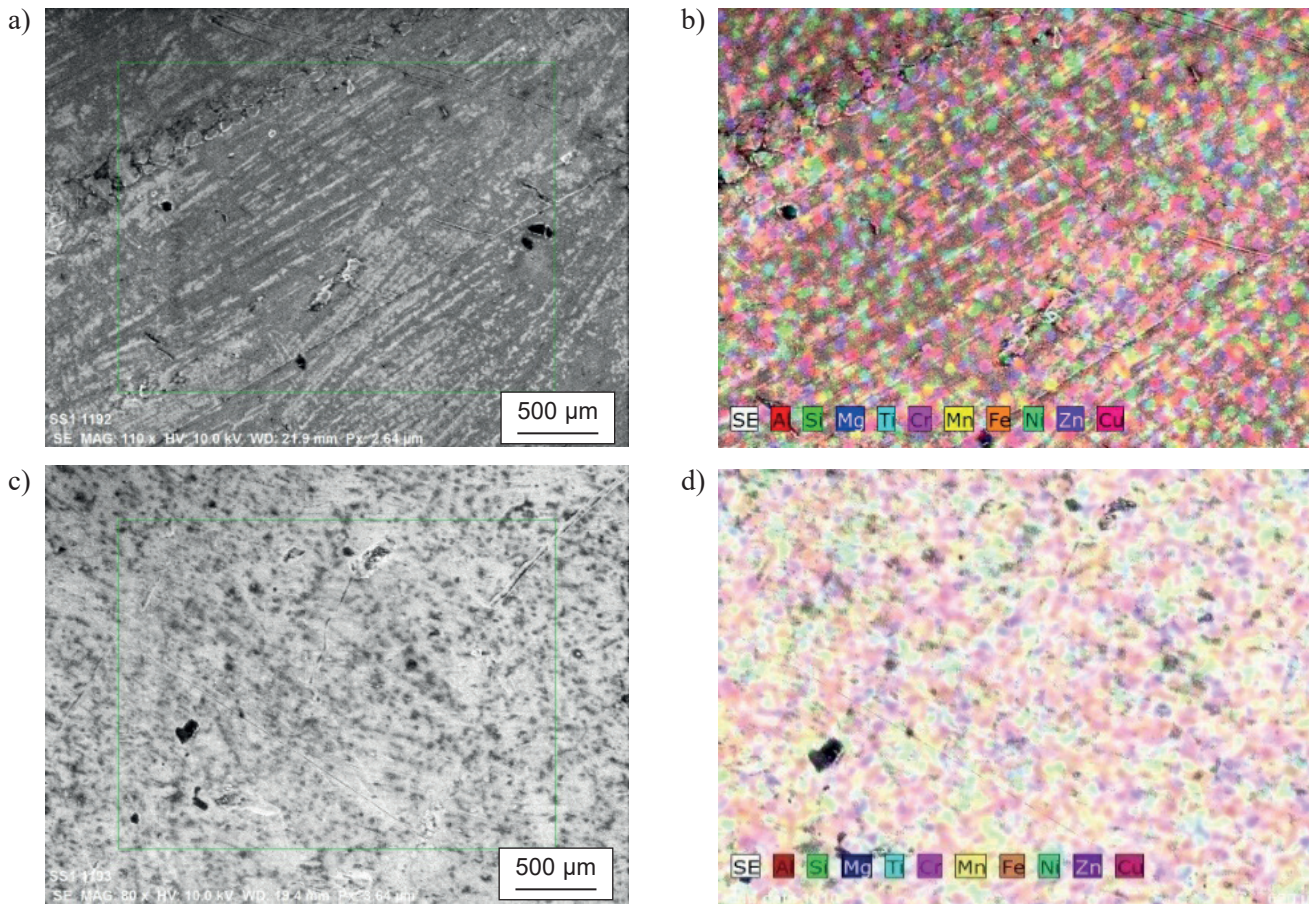
4

Bull. Pol. Ac.: Tech. 69(1) 2021, e136215

www.czasopisma.pan.pl　　PAN　　www.journals.pan.pl
POLSKA AKADEMIA NAUK

Effect of SiO2 flux on the depth of penetration, microstructure, texture and mechanical behavior of AA6063 T6 aluminum alloy using ...

Fig. 5. SEM and EDS of BM and ATIG welded samples: a, b) SEM & EDS of BM; c, d) SEM-ED Sof ATIG using SiO_2

tion of heat flow. It has good agreement with [16]. The texture study of the conventional TIG and ATIG is done using pole figures (PF). Figures 6–8 represent microstructure and PF of the samples. A cube texture ($\{001\}\langle100\rangle$) is recorded in the FZ. The main reason for this is the epitaxial growth of the columnar grains in the $\langle100\rangle$ direction. It has good agreement with [12]. The fine and equiaxed grains were found in FZ. In HAZ and PMZ recrystallization appears.

In Figs. 6 and 8 EBSD grain boundary, PF & IPF the blue represents $<111>$, green $<110>$ and red $<001>$. Figures 6 and 8 confirmed that BM grains are oriented near to $<111>$ and partly to $<001>$. In FZ of ATIG with (SiO_2) the orientation is $<001>$ and partially $<111>$. It has good agreement with [11]. In Figs. 6a, 8a and 8b, the BM have strong intensity about 25.281. In FZ intensity decreases to 4 in ATIG with (SiO_2). This reduction in intensity proved that the texture is changed
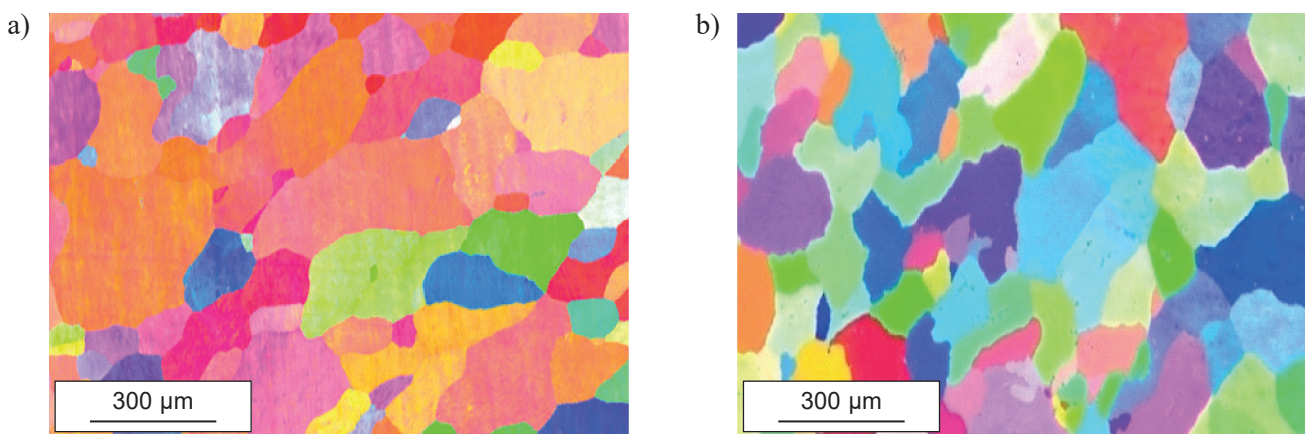

Fig. 6. EBSD grain-boundary of BM and ATIG of AA 6063-T6 using flux (SiO_2): a) EBSD of BM; b) EBSD of ATIG using SiO_2

Bull. Pol. Ac.: Tech. 69(1) 2021, e136215
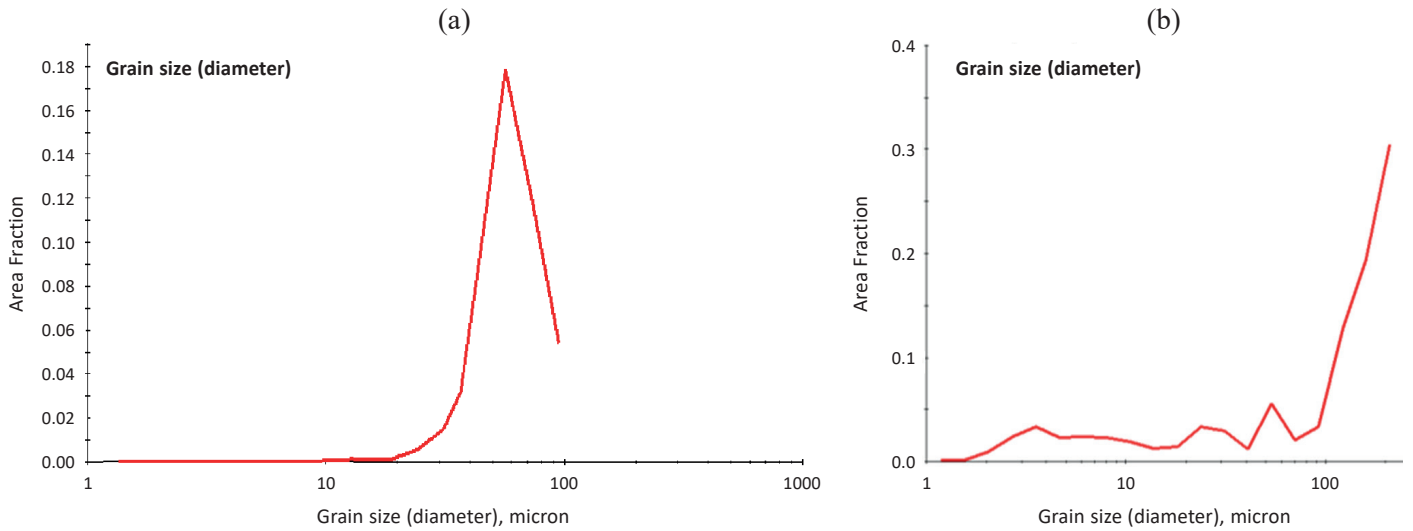
5

(a)   (b)

Fig. 7. Distribution grain size of conventional TIG and ATIG welded with flux (SiO_2): a) grain size of conventional TIG; b) grain Size of ATIG using SiO_2

in ATIG welding due to the pinning of grain boundaries by the flux (SiO_2). It is in good agreement with [14]. In Fig. 6, in the FZ of ATIG welding with flux (SiO_2) low angle grain boundaries (LAGB) and equiaxed grains are observed. Figs. 7a and 7b showed that the grain size in FZ of ATIG with flux (SiO_2) is lesser than FZ of conventional TIG [14]. In ATIG welding size of FZ and HAZ is small, therefore, there is not much change in grain size. Figure 8 represented the PF {100} [110], {111} [113] for ATIG with flux (SiO_2) and BM. It showed a symmetric texture in FZ due to uniform nucleation and plastic deforma-
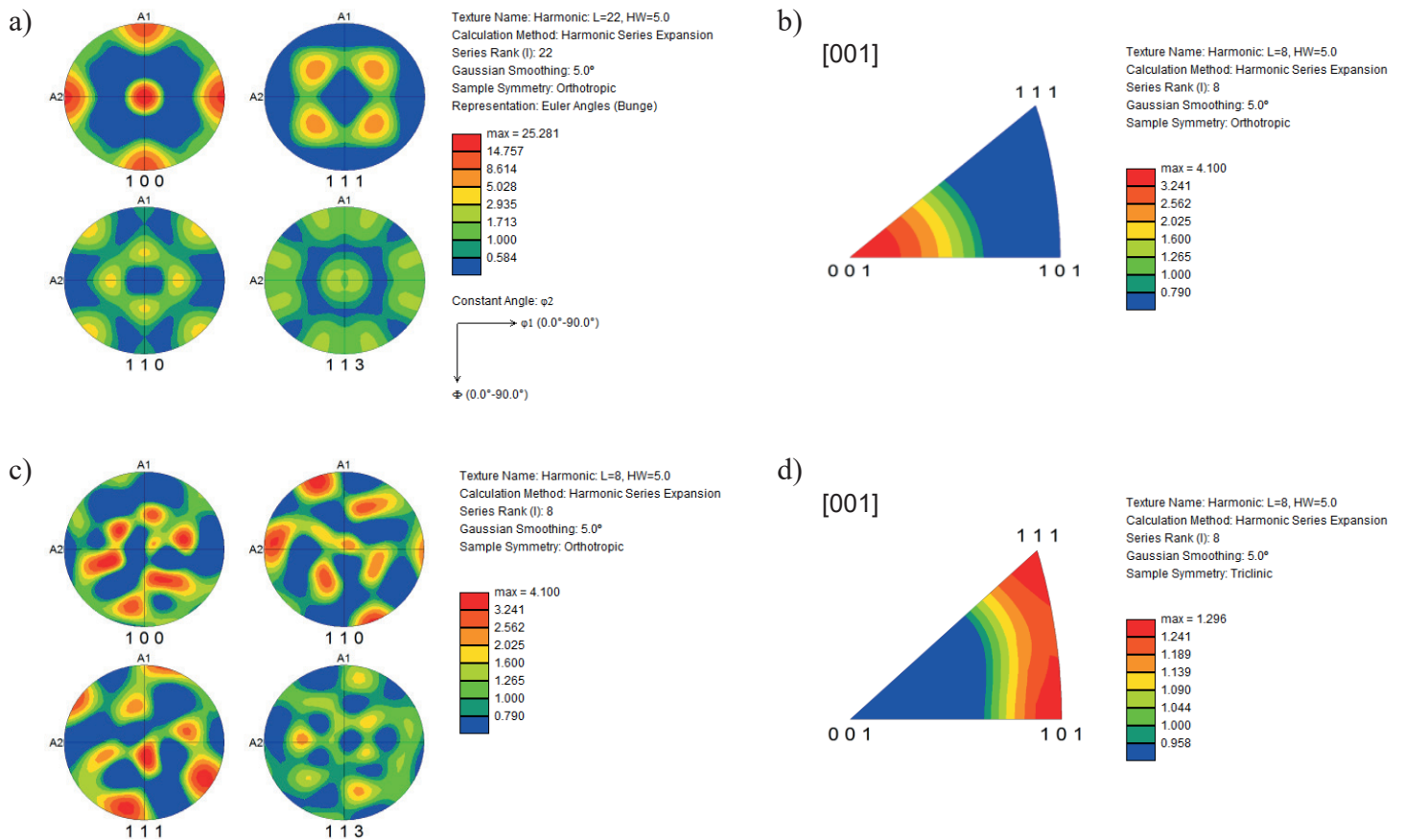

Fig. 8. PF and IPF for BM, ATIG with flux (SiO_2): a) PF for BM; b) IPF for BM; c) PF of ATIG using SiO_2; d) IPF of ATIG using SiO_2

6

Bull. Pol. Ac.: Tech. 69(1) 2021, e136215

www.czasopisma.pan.pl   PAN   www.journals.pan.pl
POLSKA AKADEMIA NAUK

Effect of SiO2 flux on the depth of penetration, microstructure, texture and mechanical behavior of AA6063 T6 aluminum alloy using ...
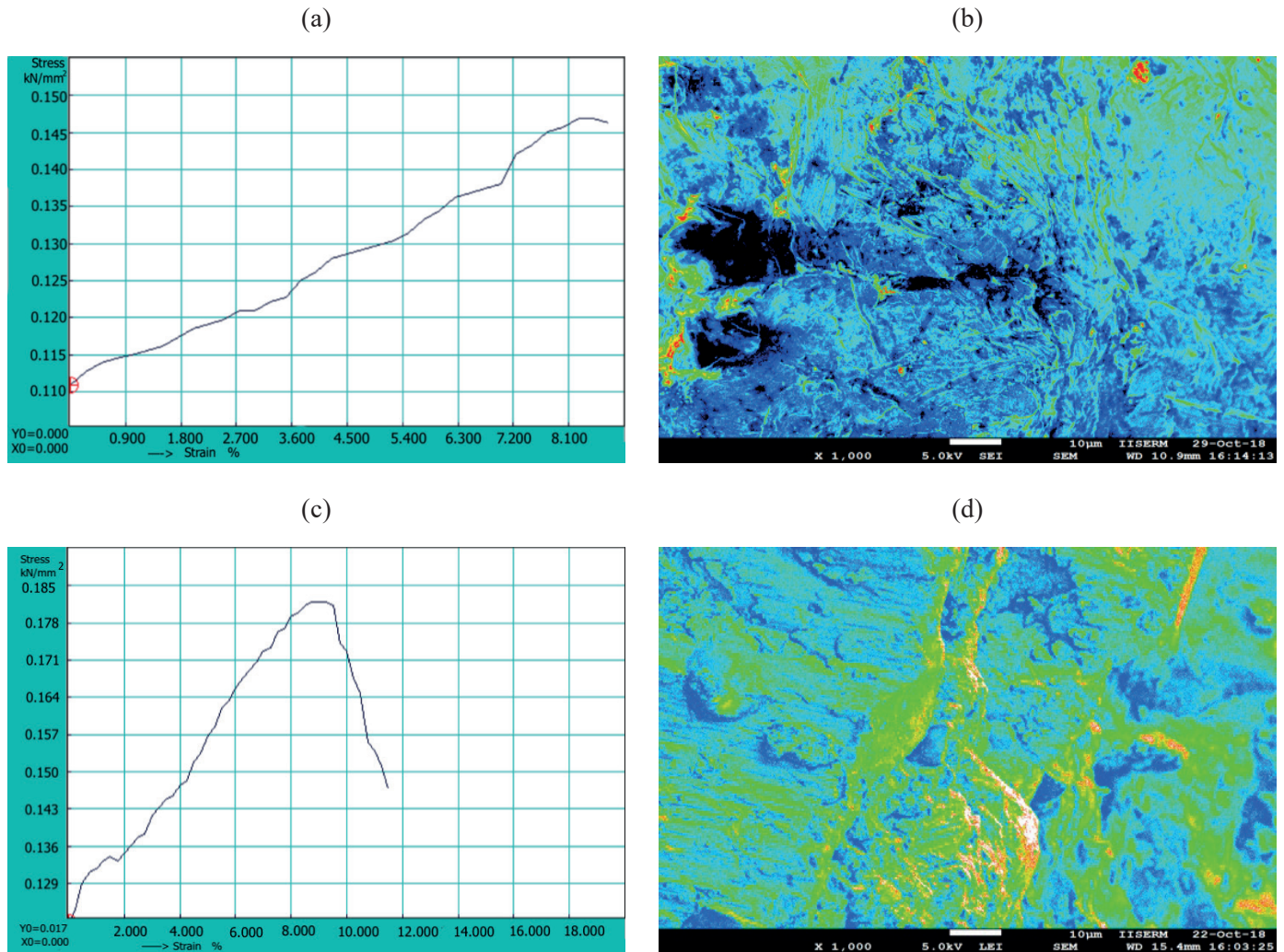
(a)

(b)

(c)

(d)

Fig. 9. Tensile and FEGSEM of a fractured specimen of conventional TIG and ATIG with flux (SiO₂): a) Stress vs Stain curve of conventional TIG; b) FEGSEM of conventional TIG; c) Stress vs Stain curve of ATIG using SiO₂; d) FEGSEM of conventional TIG

tion. In Figs. 8c and 8d, FZ region orientation is $\{001\}<100>$, $\{011\}<100>$. After the rotating by 9 degrees around A1 and 14 degrees through A2 the resultant orientation observed is $\{001\}110>$, $\{011\}<112>$, $\{110\}<223>$, $\{001\}<110>$ and $\{223\}<112>$. It is in agreement with [13–15].

3.5. Tensile strength. It is confirmed from Figs. 9a and 9c that the tensile strength of the conventional TIG and ATIG with flux (SiO₂) are 147 and 183, respectively. It is confirmed that the tensile strength of the ATIG welded joints with flux SiO₂ is greater than conventional TIG. It has good agreement with [15]. The average straining of the conventional TIG welded joints reached (8.05%) – lower than ATIG welding (12%). Figures 9a and 9b show stress-strain curves and the fracture morphology of the conventional TIG welding. Figures 9c and 9d show the stress-strain and FEGSEM fracture morphologies of ATIG welding with flux (SiO₂). It is confirmed that the ATIG welded samples are failing in ductile mode with larger fracture edges. Figure 9b confirmed that the conventional TIG sample failed without a major deformation.

The tensile samples for ATIG welding broke in PMZ. The main reason for this failure is the heterogeneous chemical composition and geometrical changes in PMZ. In the tensile fracture the parameters: dimple size, depth, and quantity are a function of the inclusions, secondary phase particle size, and spacing. An increase in the number of inclusions or secondary phase particles results in low plasticity. The ATIG had induced sufficient plastic distortion.

4. Conclusions

ATIG welding with ceramic flux (SiO₂) and conventional TIG welding of AA6063 T6 with filler AA 5356 was carried out at a constant current and gas flow rate. The influence of ceramic flux SiO₂ on the microstructure, texture, and mechanical properties was studied and the following conclusions are drawn:
- The ceramic flux in ATIG welding increased the DOP and decreased the bead width as compared to conventional TIG welding. NDE ultrasonic A-scan result of the ATIG welding

with SiO_2 confirmed the DOP in ATIG is more than in conventional TIG and welded samples are defect-free.

- The recorded tensile strength of ATIG with SiO_2 is 183 and 147MPa for conventional TIG welding. The failure mode is ductile for ATIG welding with larger fracture edges and is brittle in the case of conventional TIG welding. The average straining of the conventional TIG welded joint is lower (8.05%) than in ATIG welding (12%).
- Fine equiaxed grains exist in FZ and coarsened equiaxed grains are visible in HAZ. The width of HAZ increases with the increase of the heat input. Grain size measurements confirmed that the HAZ contains coarser grains than the BM.
- FEGSEM and EDS confirmed the presence of Fe, Mg, and Si which resulted in the formation of Al-Fe-Si intermetallic phases during solidification. Silicon combines with magnesium to form the Mg_2Si phase during the solidification. The region of the weld revealed a fully recrystallized fine grain structure.

References

[1] S. Jannet, P.K. Mathews, and R. Raja, "Comparative investigation of friction stir welding and fusion welding of 6061T6 – 5083 O aluminum alloy based on mechanical properties and microstructure", *Bull. Pol. Ac.: Tech.* 62(4), 791–795 (2014), doi: 10.2478/bpasts-2014-0086.

[2] S.T. Amancio-Filho, S. Sheikhi, J.F. dos Santos, and C. Bolfarini, "Preliminary study on the microstructure and mechanical properties of dissimilar friction stir welds in aircraft aluminium alloys 2024-T351 and 6056-T4", *J. Mater. Process. Technol.* 206. 132–142 (2008), doi: 10.1016/j.jmatprotec.2007.12.008.

[3] P. Mukhopadhyay, "Alloy Designation, Processing, and Use of AA6XXX Series Aluminium Alloys", *ISRN Metall.* 2012, 165082 (2012), doi: 10.5402/2012/165082.

[4] B. Choudhury and M. Chandrasekaran, "Investigation on welding characteristics of aerospace materials – A review", *Mater. Today Proc.* 4, 7519–7526 (2017), doi: 10.1016/j.matpr.2017.07.083.

[5] R.R. Ambriz and V. Mayagoitia, "Welding of Aluminum Alloys", in *Welding, Brazing and Soldering*, pp. 722–739, ASM International, 2018. doi: 10.31399/asm.hb.v06.a0001436.

[6] P.J. Modenesi, "The chemistry of TIG weld bead formation", *Weld. Int.* 29, 771–782 (2015), doi: 10.1080/09507116.2014.932990.

[7] A.K. Singh, V. Dey, and R.N. Rai, "Techniques to improveweld penetration in TIG welding (A review)", *Mater. Today Proc.* 4, 1252–1259 (2017), doi: 10.1016/j.matpr.2017.01.145.

[8] R.S. Vidyarthy and D.K. Dwivedi, "Activating flux tungsten inert gas welding for enhanced weld penetration", *J. Manuf. Process.* 22, 211–228 (2016), doi: 10.1016/j.jmapro.2016.03.012.

[9] R.S. Vidyarthy and D.K. Dwivedi, "Microstructural and mechanical properties assessment of the P91 A-TIG weld joints", *J. Manuf. Process.* 31, 523–535 (2018), doi: 10.1016/j.jmapro.2017.12.012.

[10] K.D. Ramkumar, V. Varma, M. Prasad, N.D. Rajan, and N.S. Shanmugam, "Effect of activated flux on penetration depth, microstructure and mechanical properties of Ti-6Al-4V TIG welds", *J. Mater. Process. Technol.* 261, 233–241 (2018), doi: 10.1016/j.jmatprotec.2018.06.024.

[11] H. Kumar and N.K. Singh, "Performance of activated TIG welding in 304 austenitic stainless steel welds", *Mater. Today Proc.* 4, 9914–9918 (2017), doi: 10.1016/j.matpr.2017.06.293.

[12] R.S. Vidyarthy, A. Kulkarni, and D.K. Dwivedi, "Study of microstructure and mechanical property relationships of A-TIG welded P91–316L dissimilar steel joint", *Mater. Sci. Eng. A.* 695, 249–257 (2017), doi: 10.1016/j.msea.2017.04.038.

[13] E.R. Imam Fauzi, M.S. Che Jamil, Z. Samad, and P. Muangjunburee, "Microstructure analysis and mechanical characteristics of tungsten inert gas and metal inert gas welded AA6082-T6 tubular joint: A comparative study", *Trans. Nonferrous Met. Soc. China (English Ed.)* 27, 17–24 (2017), doi: 10.1016/S1003-6326(17)60003-7.

[14] R.S. Coelho, A. Kostka, J.F. dos Santos, and A. Kaysser-Pyzalla, "Friction-stir dissimilar welding of aluminium alloy to high strength steels: Mechanical properties and their relation to microstructure", *Mater. Sci. Eng. A.* 556, 175–183 (2012), doi: 10.1016/j.msea.2012.06.076.

[15] A.S. Zoeram, S.H.M. Anijdan, H.R. Jafarian, and T. Bhattacharjee, "Welding parameters analysis and microstructural evolution of dissimilar joints in Al/Bronze processed by friction stir welding and their effect on engineering tensile behavior", *Mater. Sci. Eng. A.* 687, 288–297, (2017). doi: 10.1016/j.msea.2017.01.071.

[16] K.H. Dhandha and V.J. Badheka, "Effect of activatingfluxes on weld bead morphology of P91 steelbead-on-platewelds by flux assisted tungsteninert gas welding process", *J. Manuf. Process.* 17, 48–57 (2015), doi: 10.1016/j.jmapro.2014.10.004.

[17] A. Krajewski, W. Włosiński, T. Chmielewski, and P. Kołodziejczak, "Ultrasonic-vibration assisted arc-welding of aluminum alloys", *Bull. Pol. Ac.: Tech.* 60(4), 841–852 (2012), doi: 10.2478/v10175-012-0098-2.

[18] H.S. Patil and S.N. Soman, "Effect of tool geometry and welding speed on mechanical properties and microstructure of friction stir welded joints of aluminum alloys AA6082-T6", *Arch. Mech. Eng.* 61, 455–468 (2014), doi: 10.2478/meceng-2014-0026.